Anisotropic exchange in ErSb

K. Knorr, Alois Loidl, C. Vettier

Angaben zur Veröffentlichung / Publication details:

Knorr, K., Alois Loidl, and C. Vettier. 1983. "Anisotropic exchange in ErSb." *Physical Review B* 27 (3): 1769–75. https://doi.org/10.1103/physrevb.27.1769.

PHYSICAL REVIEW B VOLUME 27, NUMBER 3 1 FEBRUARY 1983

Anisotropic exchange in ErSb

K. Knorr and A. Loidl
Institut für Physik, Universität Mainz, D-6500 Mainz, Federal Republic of Germany

C. Vettier
Institut Laue-Langevin, F-38042 Grenoble Cedex, France

(Received 5 May 1982; revised manuscript received 16 August 1982)

The correlations of the magnetic moments and the magnetic order parameter of ErSb have been studied by neutron diffraction. The antiferromagnetic phase transition is of first order. The diffuse paramagnetic scattering is evaluated in terms of magnetic coupling tensors which are characterized by a strong two-ion anisotropy.

I. INTRODUCTION

Owing to their simple crystallographic structure (NaCl), the rare-earth monopnictides are presumably the best characterized of all known rare-earth compounds. A great amount of work has been done on their magnetic structures, crystal-field splittings, and magnetoelastic effects. In the last two years we have noted growing evidence that the magnetic coupling of the monopnictides is highly anisotropic. PrSb (Ref. 1) and TbP (Ref. 2) show a splitting of the paramagnetic Γ_1-Γ_4 crystal-field exciton propagating along the [100] and [110] directions. In CeSb (Ref. 3), UAs (Ref. 4), and USb (Ref. 5) the critical paramagnetic scattering was interpreted by a large difference between the longitudinal and the transverse magnetic susceptibility at the X point of the Brillouin zone.

Another interesting point is that these compounds often have a high number of components of the magnetic order parameter, a fact which may lead, within the framework of the renormalization-group theory, to first-order transitions. ErSb has been cited as a good candidate for such a behavior[6]; although the experimental results are controversial, specific-heat data[7] suggest a discontinuous transition, while previous neutron-diffraction experiments[8] suggest a continuous transition.

In this paper we report neutron-diffraction experiments on ErSb and focus our attention on the magnetic coupling in this compound, which is probed by the diffuse magnetic scattering. We will also comment on the nature of the magnetic phase transition.

II. EXPERIMENTAL

The neutron-diffraction experiments were carried out on the spectrometer D10 in a three-axis mode. It was installed at a thermal neutron guide of the high-flux reactor of the Institute Laue-Langevin. The wavelength of the incident neutrons after passing a Cu(200) monochromator was 1.97 Å. The pyrolytic-graphite (004) analyzer was set to zero energy transfer. The elastic energy resolution was 0.26 meV.

The ErSb single crystal was cut out from a polycrystalline ingot; it had a volume of 5 mm^3. The lattice constant was 6.09 Å at low temperatures. The sample was mounted in a variable-temperature cryostat with the $[0\bar{1}1]$ axis perpendicular to the scattering plane. The temperature was measured with a calibrated carbon resistor.

III. RESULTS

The neutron-diffraction measurements began with an investigation of the eight nuclear and 14 magnetic Bragg reflections in the $(0\bar{1}1)$ plane. The magnetic reflections occurred at the L points of the fcc Brillouin zone, leading to a simple type-II antiferromagnetic low-temperature phase with a propagation vector $\vec{q}_0=(\frac{1}{2},\frac{1}{2},\frac{1}{2})$. A study of the intensities, positions, and widths of the nuclear reflections showed that the chemical cell is not noticeably changed by the onset of the magnetic order. The upper limit for changes of the cell parameters is 0.1%.

An analysis of the integrated magnetic intensities, properly corrected for the Lorentz and for an isotropic Er^{3+} magnetic form factor, revealed that the spontaneous moment is perpendicular to $\vec{q}_0$ within an error of 7 deg. In a magnetic structure of this type, one expects eight domains because of the combination of four equivalent propagation vectors and the two components of the order parameter in the plane perpendicular to $\vec{q}_0$. The intensities of the magnetic Bragg reflections definitely showed that the sample did not consist of a single domain. The

low number of reflections studied did not, however, allow one to determine the statistical weights of the eight domains precisely. Therefore, it was assumed that the domains were equally populated. The R factor of this model is 14%.

The magnetic moment of the Er ions at 2.97 K is $5.5\mu_B$ or $6.8\mu_B$, depending on whether the magnetic intensities are scaled to the four strong (h,k,l all even) or the four weak (h,k,l all odd) nuclear reflections. A comparison to the weak reflections seems more appropriate, since the strong reflections might suffer from extinction effects. Following a Brillouin-type temperature dependence, one obtains a saturated moment of $(6.5-7)\mu_B$ from an extrapolation down to zero temperature. The magnetic structure is thus in good agreement with the early results of Child *et al.*[9] on a powder sample. The intensity of the magnetic $(\frac{1}{2},\frac{1}{2},\frac{1}{2})$ reflection, which can be regarded as a measure of the square of the magnetic order parameter, was studied in detail as a function of temperature (Fig. 1). One observes a hysteresis loop, centered at $T_N=3.54$ K with a width of 0.3 K, which extends up to about half the saturated intensity. First magnetic Bragg spikes, sitting on top of diffuse scattering intensities, appeared already half a degree above T_N. This behavior suggests that the transition is of first order.

The diffuse paramagnetic scattering centered at the L points was measured by performing the type of $\vec{Q}$ scans listed in Table I and indicated by solid lines in Fig. 2. After subtracting the Bragg spikes, all scan profiles are well described by Lorentzians, which are centered at the L points and superimposed on a flat background. Figures 3 and 4 show some representative scans. In the analysis, Lorentzians with a height $h(T)$ and a halfwidth $\kappa(T)$ were fitted

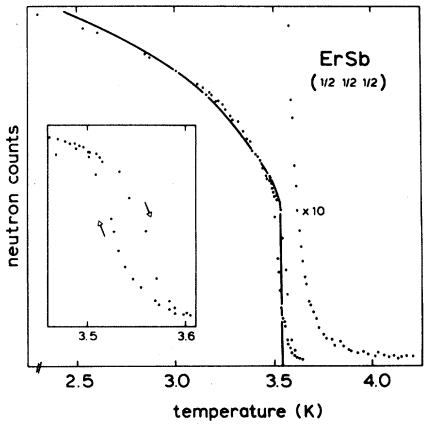

FIG. 1. Temperature dependence of the elastic intensity at the magnetic Bragg point $(\frac{1}{2},\frac{1}{2},\frac{1}{2})$. The intensity on the paramagnetic phase is expanded by a factor of 10. The inset shows the hysteresis on cooling and heating with an expanded temperature scale. The solid line is a fit to the mean-field mode described in the text.

to the data, with the Q dependence of the magnetic form factor taken into consideration. The variation of the diffuse scattering across the three-dimensional Q resolution ellipsoid was neglected since even at the lowest temperatures in the paramagnetic phase the corrections on h and κ were less than 3%. The results of this analysis are listed in Table I. Note that each scan was fitted individually. This procedure yielded slightly different values for the height of scans through the same center performed at the same temperature. Figure 5 shows the Lorentzian height and halfwidth of the diffuse intensity along the scan path $(\frac{1}{2}+2\xi,\frac{1}{2}-\xi,\frac{1}{2}-\xi)$ as a function of temperature.

TABLE I. The height h and the halfwidth κ (in reduced wave-vector units) of the Lorentzian-shaped pattern of the diffuse paramagnetic intensity at two different temperatures. a is the lattice constant.

Scan		$T=3.80$ K		$T=3.65$ K	
Center	Direction	h	κ $(2\pi/a)$	h	κ $(2\pi/a)$
$(\frac{1}{2},\frac{1}{2},\frac{1}{2})$	[211]	1320	0.09	2120	0.06
$(\frac{1}{2},\frac{1}{2},\frac{1}{2})$	[111]	1385	0.135	2208	0.10
$(\frac{1}{2},\frac{1}{2},\frac{1}{2})$	[100]	1292	0.095	2043	0.065
$(\frac{1}{2},\frac{1}{2},\frac{1}{2})$	[011]	1305	0.115	2105	0.09
$(\frac{1}{2},\frac{5}{2},\frac{5}{2})$	[100]	685	0.085	1095	0.06
$(\frac{1}{2},\frac{5}{2},\frac{5}{2})$	[011]	629	0.12	1005	0.09
$(\frac{7}{2},\frac{1}{2},\frac{1}{2})$	[100]	301	0.12	480	0.095
$(\frac{7}{2},\frac{1}{2},\frac{1}{2})$	[011]	272	0.07	435	0.06
			±0.01		±0.01

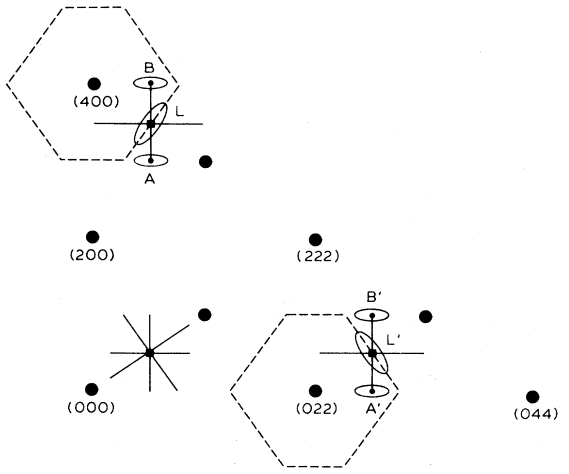

FIG. 2. Part of the (0,1,1) plane of the reciprocal space of an fcc structure. The closed circles are nuclear Bragg points. The dashed lines are the boundaries of the (4,0,0) and (0,2,2) Brillouin zones. The solid lines indicate the scans centered at three L points, which were performed for the study of the diffuse paramagnetic scattering. The ellipses schematically show the in-plane components of the susceptibility tensor $\hat{\chi}(Q)$ for $Q=A,L,B,A',L',B'$.

A. Order parameter

We address ourselves to the character of the phase transition in ErSb. As mentioned above, the renormalization-group approach predicts a first-order transition, whereas the experimental situation was controversial. One of us took part in neutron-diffraction measurements[10] which revealed a continuous transition (on a different single crystal) very

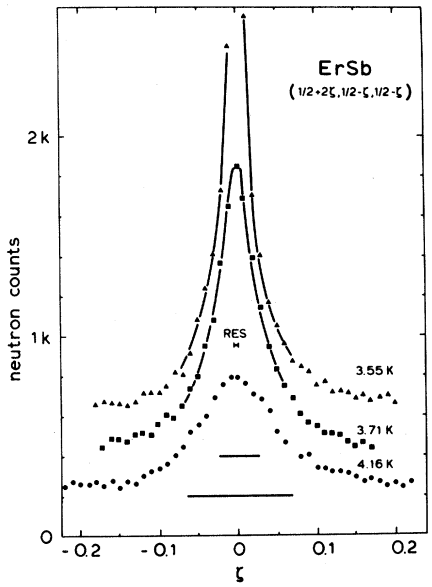

FIG. 3. Transverse Q scans through $(\frac{1}{2},\frac{1}{2},\frac{1}{2})$ at three temperatures in the paramagnetic phase. The solid lines are guides to the eye. Note the vertical offset by one or two divisions of the upper two curves. Also indicated is the instrumental Q resolution along the scan direction.

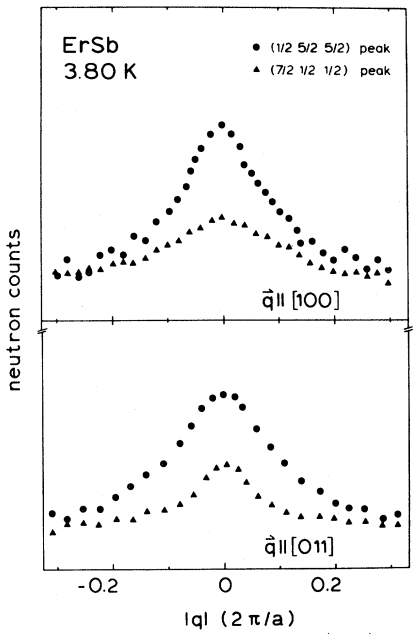

FIG. 4. Q scans of the type $\vec{Q}=\vec{Q}_0+\vec{q}$, with $Q_0=(\frac{7}{2},\frac{1}{2},\frac{1}{2})$ and $(\frac{1}{2},\frac{5}{2},\frac{5}{2})$, for $\vec{q}$ parallel to [100] and [011], respectively. Note the different widths of equivalent scans.

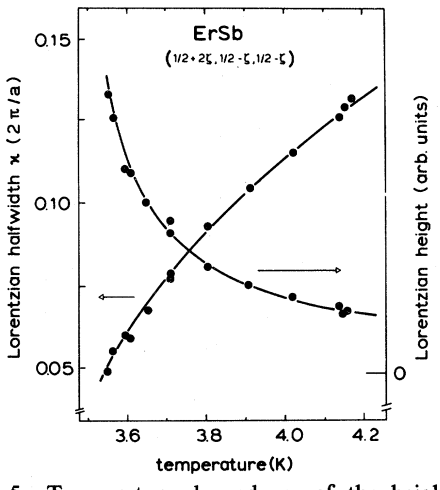

FIG. 5. Temperature dependence of the height and halfwidth of the transverse Q scans through $(\frac{1}{2},\frac{1}{2},\frac{1}{2})$ in the paramagnetic phase. The height and halfwidth were determined by fitting Lorentzians to the experimental data. The solid lines are the power laws described in the text.

similar to the results of Shapiro and Bak,[8] whereas in the present sample the onset of magnetic order is of first order. Presumably, ErSb is close to a tricritical point and sample inhomogeneities can drive the transition from first to second order.

We will show in the following that the growth of the order parameter can be alternatively explained by a magneto elastic interaction. Indications for the presence of this interaction have been brought forth by the ultrasonic study of Mullen *et al.*,[11] who observed an anomalous temperature dependence of the elastic constant c_{44}. At T_N the cell should then distort rhombohedrally. So far, however, there is no direct evidence for a structural phase transition in ErSb.

A mean-field calculation similar to that of Ray and Sivardiere[12] on CeAg was carried out, where in addition to the magnetic coupling an electric quadrupole coupling between the Er $4f$ states was considered. For simplicity the crystal-field level scheme was truncated to the $\Gamma_8^{(1)}$ ground state. The quantization was performed not along the easy [111] axis, but along [110] in order to simulate a spin direction perpendicular to the propagation vector of the magnetic structure. An excellent verification (see Fig. 1, solid line) of the onset of the magnetic order parameter could be achieved by adjusting the two coupling parameters in the following way: The magnetic coupling was chosen to yield a magnetic ordering in the absence of quadrupole effects at 3.43 K, which is the Neél temperature extrapolated from diffuse scattering in the paramagnetic phase. Note that the magnetic dipole and electric quadrupole susceptibilities are decoupled in the paramagnetic state. The quadrupolar coupling is set to induce a structural ordering in the absence of magnetic interactions at a fictitious temperature of 2.1 K, since then the actual transition is predicted to be of first order at 3.53 K due to a simultaneous ordering of the magnetic dipoles and the electric quadrupoles.

A choice between the alternative explanations for the first-order phase transition—renormalization-group considerations or magnetoelastic effects—can be made on the basis of studies of these compounds under hydrostatic and uniaxial pressure along the [111] axis, since the order parameter reacts differently with respect to the two types of pressure in the two models. In MnO, which has the same magnetic structure as ErSb, this kind of experiment favored an interpretation based on renormalization-group theory, even in the presence of strong magnetoelastic interactions.[13]

B. Diffuse scattering

A comparison of the reciprocal Q widths of the diffuse scattering with the Er-Er distances suggests that the measurements in the paramagnetic phase are well above the critical regime. In fact, the Lorentzian components of the transverse scans through $(\frac{1}{2},\frac{1}{2},\frac{1}{2})$ follow power laws of the form $h\sim(T-T_N')^{-\gamma}$ and $\kappa\sim(T-T_N'')^{\nu}$, with exponents $\gamma=1.0\pm0.1$ and $\nu=0.50\pm0.02$, and $T_N'=3.41\pm0.02$ K, $T_N''=3.45\pm0.02$ K (solid lines of Fig. 3). These "extrapolated paramagnetic critical temperatures" are significantly lower than the actual transition temperature $T_N=3.54$ K. Thus the discontinuous onset of the magnetic ordering suppresses the evolution of critical fluctuations.

The mean-field values of the exponents propose an analysis of the paramagnetic scattering in terms of a mean-field—random-phase-approximation model. Here the full magnetic susceptibility tensor is given by

$$\hat{\chi}(\vec{Q})=\chi_0[\hat{1}+\hat{J}(\vec{Q})\chi(\vec{Q})]\,, \tag{1}$$

where $\hat{J}(\vec{Q})$ is the Fourier transform of the magnetic coupling tensor, and χ_0 is the scalar susceptibility of a single Er^{3+} ion in the cubic crystal field. χ_0 can be calculated from the crystal-field parameters of ErSb, which have been obtained from data on inelastic neutron scattering.[8] At the low temperatures, which are of interest here, χ_0 can be approximated by

$$\chi_0=g^2\mu_B^2(14.5/T+0.359)\,. \tag{2}$$

The first term represents the Curie contribution of the $\Gamma_8^{(1)}$ ground state, the second one is due to the crystal-field transitions out of the ground state, in particular $\Gamma_8^{(1)}\rightarrow\Gamma_8^{(2)}$. The neutron scattering cross section for magnetic scattering is related to the susceptibility $\hat{\chi}$ by

$$\frac{d\sigma}{d\Omega}\sim f^2(\vec{Q})T\sum_{\alpha,\beta}\left[\delta_{\alpha\beta}-\frac{Q_\alpha Q_\beta}{Q^2}\right]\chi_{\alpha\beta} \qquad (\alpha,\beta=x,y,z)\,. \tag{3}$$

This form is valid for energy-integrated scattering, its application to the present problem introduces only minor errors since the elastic components of the susceptibility are at least 1 order of magnitude stronger than the inelastic crystal-field transitions.

In rare-earth systems it is standard practice to regard the exchange interaction as isotropic. In that case, $\hat{\chi}(\vec{Q})$ of a cubic structure reduces to a scalar quantity, with the consequence that the pattern of the diffuse scattering is identical in every Brillouin zone, apart from variations due to the form factor. In the present experiment, however, we observed different profiles for equivalent scans through the three L points investigated (Fig. 4 and Table I). To be specific, equivalent scans, e.g., the three along (100),

have different widths, the diffuse intensities at $(\frac{7}{2},\frac{1}{2},\frac{1}{2})$ and $(\frac{1}{2},\frac{5}{2},\frac{5}{2})$ deviate by a factor of more than 2, though the value of $|\vec{Q}|$ is identical. (An anisotropic form factor, which might explain the mismatch of the intensities, could not be observed in the analysis of the magnetic structure.)

We interpret these findings by a two-ion anisotropy of the magnetic coupling. For an insight into the nature of the anisotropy we consider the most general form of a coupling to the first and second Er neighbors which is compatible with the fcc lattice formed by the Er ions. A treatment of this type was already applied by us[2,14] on the dispersion of the paramagnetic excitations of TbP and PrSb and later used by Sinha *et al.*[4] for an interpretation of the diffuse scattering in UAs. The coupling tensors between the ion at the origin and a first neighbor at $(a/2,a/2,0)$ or a second neighbor at $(a,0,0)$ are, respectively, of the form

$$\hat{J}_1=\begin{bmatrix}\alpha_1 & \gamma_1 & 0\\ \gamma_1 & \alpha_1 & 0\\ 0 & 0 & \beta_1\end{bmatrix},\quad \hat{J}_2=\begin{bmatrix}\alpha_2 & 0 & 0\\ 0 & \beta_2 & 0\\ 0 & 0 & \beta_2\end{bmatrix}. \tag{4}$$

The coupling to the other first and second neighbors is obtained by applying the cubic-symmetry operations. The components of the Fourier-transformed J tensor are then given by

$$\begin{aligned}J_{\alpha\alpha}(\vec{Q})&=2\alpha_2\cos(aQ_\alpha)+2\beta_2[\cos(aQ_\beta)+\cos(aQ_\gamma)]\\&\quad+2\alpha_1\{\cos[\tfrac{1}{2}a(Q_\alpha+Q_\beta)]+\cos[\tfrac{1}{2}a(Q_\alpha-Q_\beta)]+\cos[\tfrac{1}{2}a(Q_\alpha+Q_\gamma)]+\cos[\tfrac{1}{2}a(Q_\alpha-Q_\gamma)]\}\\&\quad+2\beta_1\{\cos[\tfrac{1}{2}a(Q_\beta+Q_\gamma)]+\cos[\tfrac{1}{2}a(Q_\beta-Q_\gamma)]\},\\J_{\alpha\beta}(\vec{Q})&=2\gamma_1\{\cos[\tfrac{1}{2}a(Q_\alpha+Q_\beta)]-\cos[\tfrac{1}{2}a(Q_\alpha-Q_\beta)]\},\quad \alpha\neq\beta .\end{aligned} \tag{5}$$

$\hat{\chi}(\vec{Q})$ and $d\sigma/d\Omega$ can be now calculated from Eqs. (1)–(3). A series expansion of $d\sigma/d\Omega$ around the L point leads to Lorentzian-shaped profiles of diffuse intensity whose height and width follow the mean-field power laws from above.

An application of this model failed insofar as the theoretical values for the Q widths of the diffuse scattering pattern were always larger than the experimental results for reasonable choices of the ordering temperature. Obviously, the actual range of the magnetic interaction is longer than assumed here. Nevertheless, a comparison of the model and the experiment should give valuable information on the anisotropy of the interaction, which is expected to be dominated by the coupling to first and second neighbors as shown in the isomorphic compound TbP.

In detail we come to the following conclusions:

(i) Exactly at the L point, $\hat{J}(Q)$ is sensitive to the off-diagonal element γ_1 and to the combination $\alpha_2+2\beta_2$ of the second-neighbor elements α_2 and β_2, only. If γ_1 would vanish the susceptibility at the L points were isotropic and would diverge at a temperature proportional to $\alpha_2+2\beta_2$. Finite values of γ_1 lead to an anisotropic $\hat{\chi}(L)$ tensor and hence to different intensities at different L points, in particular to different intensities at $\vec{Q}=(\frac{7}{2},\frac{1}{2},\frac{1}{2})$ and $(\frac{1}{2},\frac{5}{2},\frac{5}{2})$ (a conclusion which will be made plausible further below). The intensity ratio observed for these two L points requires $\gamma_1>0$, which means that the transverse susceptibility is larger and diverges at a higher temperature than the longitudinal susceptibility ($T_N^{\text{trans}}>T_N^{\text{long}}$). This result is in agreement with the structure of the antiferromagnetic phase where the spontaneous moment is at a right angle with the propagation vector. A quantitative analysis yields that $T_N^{\text{trans}}-T_N^{\text{long}}$ is about 0.6 K. A comparison of this temperature difference with the actual ordering temperature suggests that γ_1 is an order of magnitude smaller than $\alpha_2+2\beta_2$.

(ii) The Q width of scans along [100] depends on the diagonal elements of the second-neighbor coupling tensor α_2 and β_2, only. The differences of the widths along this direction at the three L points investigated yield that α_2 is about twice as large as β_2 with α_2 and β_2 both negative.

(iii) The diagonal elements of the first-neighbor coupling tensor α_1 and β_1 can be adjusted using the results of the other scans. β_1 is about three times larger than α_1, with α_1 and β_1 being both positive.

A qualitative understanding for the different heights and halfwidth of equivalent scans can be obtained from Fig. 2, which shows a part of the $(0\bar{1}1)$ plane of the reciprocal space.

We compare the scans along the [100] direction through the L points $(\frac{7}{2},\frac{1}{2},\frac{1}{2})$ and $(\frac{1}{2},\frac{5}{2},\frac{5}{2})$ (paths A-L-B and A'-L'-B'). From the model the susceptibility tensor $\hat{\chi}(\vec{Q})$ is calculated along the scan path. The tensor is especially simple for the center points and the end points, here the in-plane components of the $\hat{\chi}$ tensors are shown schematically as ellipses.

[The length of a radius vector of the ellipse centered at $\vec{Q}$ is a measure of $\hat{\chi}(\vec{Q})$ along the direction specified by the vector.] At L and L', the two long axes of the ellipsoid have equal length and they are perpendicular to the reduced wave vector $\vec{q}$; the short axis is parallel to $\vec{q}$. This difference between the transverse χ_T and the longitudinal χ_L susceptibility is entirely due to the off-diagonal element γ_1. We know from above that χ_T is 0.6 K ahead of χ_L, the ratio χ_T/χ_L grows when approaching T_N. It is calculated to be about 2 at 4 K and 6 at T_N. When leaving the L points, the principal axes of the χ tensor change. Their directions no longer correspond to pure polarizations, and the residual degeneracy of the lengths of two axes is lifted. Along the [100] direction, these effects are due to the difference $\alpha_2-\beta_2$ of the second-neighbor diagonal elements. At the points A,B,A',B' the polarizations are pure again. The in-plane transverse axis is now the shortest one, and the out-of-plane transverse axis is slightly longer than the longitudinal axis.

The different scan profiles along A-L-B and A'-L'-B' result from the scattering geometry. The scattered intensity is proportional to the average length of the cuts through the χ ellipsoids perpendicular to the full wave vector $\vec{Q}$. It is evident from Fig. 2 that this cut at L' is longer than at L; hence the intensity at L' is higher than at L. The situation is reversed at the end points of the scans; here the cuts at A' and B' are shorter than at A and B. Thus the scattered intensity starts at high values at L' and drops to very low values at A' and B', whereas the intensity variations along A-L-B are much smaller. This behavior is reflected in the heights and halfwidths of Table I.

The model introduces two sorts of anisotropy, the differences in the diagonal elements $\alpha_1-\beta_1$ and $\alpha_2-\beta_2$ and the off-diagonal element γ_1. Referring to the differences $\alpha_i-\beta_i$, we consider a pair of Er next neighbors with a bond along the diagonal of the (x,y) plane. The results of the present study demand that the coupling of the components of the magnetic moments perpendicular to this plane is three times stronger than the coupling of the components in the plane. For the second-neighbor bonds the components along the bonds are twice as strongly coupled as the components perpendicular to the bond. It is surprising that for first-neighbor bonds the bond plane determines the anisotropy, whereas for second neighbors it is the bond direction which determines it. This fact rules out that the coupling is due to the same multipolar type of interaction for first and second neighbors. It rather emphasizes the importance of the nonmagnetic Sb ions. Presumably, the exchange is mediated by the Sb valence electrons. In this view, the exchange paths between the pair of first Er neighbors at (0,0,0) and $(a/2,a/2,0)$ lie within the (x,y) plane and perform right angles passing across the Sb ions at $(a/2,0,0)$ and $(0,a/2,0)$, whereas second Er neighbors would be connected by a linear path across the Sb ion halfway in between.

The same type of highly anisotropic interaction tensors were obtained for the isomorphic compounds PrSb, TbP, USb, UAs, and CeSb. In the Ce and U monopnictides the experimental evidence came— as in the present work—from the pattern of the diffuse intensity in the vicinity of the ordering wave vector, whereas in the two singlet–ground-state systems PrSb and TbP the anisotropic coupling $J(\vec{Q})$ was determined along the main symmetry directions from the dispersion of the split Γ_1-Γ_4 excitation. The results on the two latter compounds and the relations of the parameters in ErSb show that the strongest mismatch between the longitudinal and the transverse susceptibility occurs around the X point of the Brillouin zone, which happens to become the critical wave vector in CeSb, USb, and UAs, where in fact the transverse components were almost completely suppressed. Comparing the elements $\alpha_1,\beta_1,\alpha_2,\beta_2$ of ErSb and the neighboring compound TbP,[14] one notes that the signs are identical and that $\beta_1>\alpha_1$ in both cases, but that the inequality between α_2 and β_2 is reversed.

In addition to the results on the other compounds, we could probe the small off-diagonal coefficient γ_1 in ErSb. This was possible since the other sources of anisotropy vanish at the L point. Presumably, it is correct to regard γ_1 as being due to the classical dipole-dipole interaction, since this coupling is estimated to have the right strength and has the appropriate symmetry. The dipole-dipole coupling tensor to the first neighbor at $(a/2,a/2,0)$ is of the form

$$\begin{pmatrix} \epsilon & \epsilon & 0 \\ \epsilon & \epsilon & 0 \\ 0 & 0 & 0 \end{pmatrix}.$$

Since all the compounds mentioned are isomorphic, the common type of anisotropic coupling is expected to be intimately related to the specific crystallographic structure. As mentioned above, the symmetry of the coupling tensors suggests that the magnetic interaction is guided by the nonmagnetic neighbors of the magnetic ion. The microscopic origin—be it superexchange, covalent bonding, or s-f mixing—is yet unclear. In any case, the anisotropy should increase, as observed in the compounds, with the spatial extent of the f subshell; the effect is, however, not reserved to the anomalous f ions Ce and U.

ACKNOWLEDGMENTS

We thank E. Bucher and B. Lüthi for providing us with the sample. The work was supported by the Bundesminister für Forschung und Technologie.

[1]C. Vettier, D. B. McWhan, E. I. Blount, and G. Shirane, Phys. Rev. Lett. 39, 1028 (1977).

[2]A. Loidl, K. Knorr, J. K. Kjems, and B. Lüthi, Z. Phys. B 35, 253 (1979).

[3]B. Hälg, A. Furrer, W. Hälg, and O. Vogt, Z. Phys. C 14, L969 (1981).

[4]S. K. Sinha, G. H. Lander, S. M. Shapiro, and O. Vogt, Phys. Rev. B 23, 4556 (1981); Phys. Rev. Lett. 45, 1028 (1980).

[5]G. H. Lander, S. K. Sinha, D. M. Sparlin, and O. Vogt, Phys. Rev. Lett. 40, 523 (1978).

[6]P. Bak, S. Krinsky, and D. Mukamel, Phys. Rev. Lett. 36, 52 (1976).

[7]F. Hulliger and B. Natterer, Solid State Commun. 13, 221 (1973).

[8]S. M. Shapiro and P. Bak, J. Phys. Chem. Solids 36, 579 (1975).

[9]H. R. Child, M. K. Wilkinson, J. W. Cable, W. C. Koehler, and E. O. Wollan, Phys. Rev. 131, 922 (1963).

[10]J. Kötzler, W. Joswig, and K. Knorr (unpublished).

[11]M. E. Mullen, B. Lüthi, P. S. Wang, E. Bucher, L. D. Longinotti, J. P. Maita, and H. R. Ott, Phys. Rev. B 10, 186 (1974).

[12]D. K. Ray and J. Sivardiere, Solid State Commun. 19, 1053 (1976).

[13]D. Bloch and C. Vettier, J. Magn. Magn. Mater. 15-18, 589 (1980).

[14]K. Knorr, A. Loidl, and J. K. Kjems, in *Crystalline Electric Field Effects and Structural Effects in f-Electron Systems,* edited by J. E. Crow, R. P. Guertin, and T. W. Mihalisin (Plenum, New York, 1980), p. 141.